different geometry from that described by Watson and Crick (Fig. 1a, b). Similarly, an alternative base-pairing geometry can occur for G•C pairs. Hoogsteen pointed out that if the alternative hydrogen-bonding patterns were present in DNA, then the double helix would have to assume a quite different shape. Hoogsteen base pairs are, however, rarely observed.

Nikolova and colleagues' key finding[1] is that, in some DNA sequences, especially CA and TA dinucleotides, Hoogsteen base pairs exist as transient entities that are present in thermal equilibrium with standard Watson–Crick base pairs. The detection of the transient species required the use of NMR techniques that have only recently been applied to macromolecules[6].

Why is this finding important? Hoogsteen base pairs have, after all, previously been observed in protein–DNA complexes[7–9] (Fig. 1c). But it has not been possible to determine whether Hoogsteen base pairs are present in free DNA. Nikolova and colleagues' study[1] reveals that the ability to flip between Watson–Crick and Hoogsteen base pairing in free DNA is an intrinsic property of individual sequences. This implies that some proteins have evolved to recognize only one base-pair type, and use intermolecular interactions to shift the equilibrium between the two geometries[9].

DNA has many features that allow its sequence-specific recognition by proteins. This recognition was originally thought to primarily involve specific hydrogen-bonding interactions between amino-acid side chains and bases. But it soon became clear that there was no identifiable one-to-one correspondence — that is, there was no simple code to be read. Part of the problem is that DNA can undergo conformational changes that distort the classical double helix. The resulting variations in the way that DNA bases are presented to proteins can thus affect the recognition mechanism.

More significantly, it has become evident that distortions in the double helix are themselves dependent on base sequence. This enables proteins to recognize DNA shape in a manner reminiscent of the way that they recognize other proteins and small ligand molecules. For example, stretches of A and T bases can narrow the minor groove of DNA (the narrower of the two grooves in the double helix), thus enhancing local negative electrostatic potentials and creating binding sites for appropriately placed, positively charged arginine amino-acid residues[3].

Nikolova and colleagues' discovery[1] that DNA base pairs can so easily leave their favoured Watson–Crick conformation comes as a surprise. But viewed in another way, the phenomenon is not so different from protein side chains undergoing a conformational change so as to optimize binding with another protein. The real surprise where DNA is concerned is that the constraints of the double helix don't preclude this possibility. The presence of Hoogsteen base pairs in detectable amounts — even in free DNA — therefore provides a notable example of the remarkable plasticity of the canonical double helix. It also implies that, if DNA bases are regarded as letters, each letter potentially has two meanings that determine both hydrogen-bonding patterns and structural variations in the double helix.

Structural biologists have long recognized that there is no second code in which certain amino acids recognize complementary DNA bases in protein–DNA interactions. Nevertheless, protein–DNA binding is still commonly thought of purely in terms of codes and sequence motifs, rather than as the binding of two large macromolecules that have complex shapes and considerable conformational flexibility[10]. Nikolova and colleagues' discovery reminds us that DNA offers proteins not only an enticing linear alphabet, but also a set of conformations that can be recognized in a sequence-dependent way. Understanding how the linear sequence of bases in DNA is recognized by proteins is therefore a problem that must be solved in three dimensions. This will require structural, biochemical, genomic and computational studies on both naked double helices and protein–DNA complexes. ■

Barry Honig *is at the Howard Hughes Medical Institute, Center for Computational Biology and Bioinformatics, Department of Biochemistry and Molecular Biophysics, Columbia University, New York, New York 10032, USA.* **Remo Rohs** *is in the Molecular and Computational Biology Program, Department of Biological Sciences, University of Southern California, Los Angeles, California 90089, USA.*
e-mails: bh6@columbia.edu; rohs@usc.edu

1. Nikolova, E. N. *et al. Nature* **470,** 498–502 (2011).
2. Parker, S. C. J., Hansen, L., Abaan, H. O., Tullius, T. D. & Margulies, E. H. *Science* **324,** 389–392 (2009).
3. Rohs, R. *et al. Nature* **461,** 1248–1253 (2009).
4. Watson, J. D. & Crick, F. H. C. *Nature* **171,** 737–738 (1953).
5. Hoogsteen, K. *Acta Crystallogr.* **16,** 907–916 (1963).
6. Palmer, A. G. & Massi, F. *Chem. Rev.* **106,** 1700–1719 (2006).
7. Aishima, J. *et al. Nucleic Acids Res.* **30,** 5244–5252 (2002).
8. Nair, D. T., Johnson, R. E., Prakash, S., Prakash, L. & Aggarwal, A. K. *Nature* **430,** 377–380 (2004).
9. Kitayner, M. *et al. Nature Struct. Mol. Biol.* **17,** 423–429 (2010).
10. Rohs, R. *et al. Annu. Rev. Biochem.* **79,** 233–269 (2010).
11. Chen, Y., Dey, R. & Chen, L. *Structure* **18,** 246–256 (2010).

CLIMATE CHANGE

Old droughts in New Mexico

A long climate record reveals abrupt hydrological variations during past interglacials in southwestern North America. These data set a natural benchmark for detecting human effects on regional climates. SEE LETTER P.518

JOHN WILLIAMS

Southwestern North America is a pretty dry place, and is likely to get drier this century because of anthropogenic climate warming. On page 518 of this issue[1], Fawcett *et al.* provide a climate record from deep in the past that will help in assessing the future hydrological regime for the area.

Climate models consistently project declines in winter precipitation for the southwest, in response to rising greenhouse gases as the subtropical dry zones expand polewards[2,3]. This precipitation decline, combined with expected increases in evaporation rates and reduced snowpack, would severely strain the region's capacity to adapt to climate change. Moreover, the southwest is historically prone to droughts, with six multi-year droughts in the nineteenth and twentieth centuries, including the infamous 1930s Dust Bowl[4]. These droughts are linked to yearly-to-decadal variations in sea surface temperatures in the tropical Pacific, enhanced by local soil-moisture feedbacks[5]. Further understanding of the mechanisms of hydrological variability, together with efforts to limit societal vulnerability to climate change, are priorities in global-change research[4].

Palaeoclimatic studies have made an essential, if not particularly reassuring, contribution to this effort, by providing insight into the natural behaviour of hydrological systems and a longer-term context for historical and projected changes. Tree-ring records offer sobering evidence of widespread and decades-long 'megadroughts' in the western United States over the past several millennia that dwarfed recorded historical droughts[6]. Records spanning the past 11,000 years (the Holocene interglacial) demonstrate long-term shifts in southwestern monsoon


D. USNER

Figure 1 | An aerial view of Valles Caldera, site of the lake sediments from which Fawcett *et al.*[1] extracted their climate record.

intensity[7]. Fawcett *et al.*[1] now present a beautifully detailed record of climatic variability between 370,000 and 550,000 years ago from lake sediments at Valles Caldera, New Mexico (Fig. 1). This time interval spans two earlier interglacial periods, known as Marine Isotope Stage (MIS) 11 and 13.

Among palaeoclimatic aficionados, MIS 11 is of great interest, because Earth's orbital configuration, and hence the insolation regime (amount of solar radiation reaching Earth), closely resembles that during the Holocene[8]. Usually, interglacial periods are short, lasting half of one precessional cycle (about 10,000 years), and end when summer cooling in the Northern Hemisphere triggers a new round of continental glaciations. However, during MIS 11, Earth's orbit was nearly circular for an unusually long time, dampening the effect of precessional variations on seasonal insolation and causing MIS 11 to last 50,000 years. (MIS 13 is comparably long and hence also of interest.) The similar orbital configuration today raises the fascinating possibility that, even without rising greenhouse gases, the current interglacial might have another 40,000 years to go[9]. Thus, palaeoclimatic records from MIS 11 offer unique insights into the potential trajectory for the contemporary climate system, in the absence of humanity's effects.

Unfortunately, most MIS 11 records are from Antarctic ice cores or marine sediments; terrestrial records are scarce. The Valles Caldera record is remarkable for the wealth of palaeoclimatic proxy data collected by Fawcett and colleagues[1]. The proxies include both new geochemical indicators of past temperatures and tried-and-true proxies for terrestrial vegetation (pollen and $\delta^{13}C$ [$^{13}C/^{12}C$]), lake productivity (silica/titanium ratios) and lake hydrology (total organic carbon and calcium concentrations). The age model is well constrained by a basal, radiometrically dated ash layer and by palaeomagnetic reversals of known age, and the temporal resolution is fine enough to resolve millennial-scale climate variations.

The Valles Caldera record reveals three warm and two cool stages within MIS 11, with a 2 °C difference between stages. Warm peaks probably correspond to peaks in summer insolation.

The first warm stage (MIS 11e) is the counterpart to the past 11,000 years, and its trajectory is documented in exquisite detail. MIS 11e began with a rapid 8 °C warming, increased abundances of vegetation such as oak and juniper that prefer warm conditions, and increased lake productivity. A few thousand years later, abundances of grasses with the C_4 photosynthetic system increased, suggesting warm and at least seasonally wet conditions. Simultaneously, however, the Valles Caldera lake became hydrologically closed (there were no outflowing streams), a signal of negative water balance. This somewhat paradoxical result can be explained by differing seasonal precipitation signals, with the C_4 grasses responding to continued summer precipitation and lake hydrology responding to reduced winter precipitation. Summer and winter precipitation also diverged during the early Holocene, probably due to the effects of insolation on southwestern monsoon intensity[10].

The next phase within MIS 11e is the most striking: abrupt shifts in $\delta^{13}C$ and lowered total organic carbon suggest a rapid collapse of C_4 grasses and oxidation of lake sediments; mud cracks in the sediments show that the lake dried out. This arid episode lasted several thousand years, and apparently began and ended abruptly. At least two other multi-millennial dry periods occurred during MIS 11, and higher-frequency variations in total organic carbon and $\delta^{13}C$ hint at sub-millennial hydrological variability during the warm stages of MIS 11.

Mud cracks and low total organic carbon also characterize much of MIS 13, implying that this interglacial was similarly marked by recurring episodes of high temperatures and aridity. Interestingly, MIS 13 seems to have been warmer and drier than MIS 11, despite lower concentrations of atmospheric carbon dioxide and methane during MIS 13 (refs 11, 12). This suggests that the larger variations in insolation during MIS 13 strongly regulated southwestern aridity.

What lessons can we draw from the Valles Caldera record? First, in southwestern North America, hydrological variability seems to be the rule rather than the exception during interglacial periods. Second, on timescales of 10^3 to 10^4 years, orbital precession strongly influences southwestern monsoon intensity and seasonal precipitation. Third, insofar as MIS 11 is a good analogue for the Holocene, we should now be at a time roughly equivalent to the transition between warm MIS 11e and cool MIS 11d. If so, southwestern climates might naturally be trending towards a somewhat cooler and wetter stage — except that other factors (us) are affecting climate. Knowing the likely natural trends thus helps us to diagnose the causes of twenty-first-century hydrological trends. And perhaps, just perhaps, these natural trends will partially mitigate the projected drying in the southwest. ■

John (Jack) Williams *is in the Department of Geography and Center for Climatic Research, University of Wisconsin-Madison, Madison, Wisconsin 53706-1695, USA.*
e-mail: jww@geography.wisc.edu

1. Fawcett, P. J. *et al. Nature* **470,** 518–521 (2011).
2. Intergovernmental Panel on Climate Change *Climate Change 2007: The Physical Science Basis* (Cambridge Univ. Press, 2007).
3. Seager, R. & Vecchi, G. A. *Proc. Natl Acad. Sci. USA* **107,** 21277–21282 (2010).
4. Cook, E. R. *et al.* in *Abrupt Climate Change. A Report by the U.S. Climate Change Science Program and the Subcommittee on Global Change Research* (eds Clark, P. U. *et al.*) 143–257 (US Geol. Surv., 2008).
5. Schubert, S. D., Suarez, M. J., Pegion, P. J., Koster, R. D. & Bacmeister, J. T. *Science* **303,** 1855–1859 (2004).
6. Cook, E. R., Seager, R., Cane, M. A. & Stahle, D. W. *Earth Sci. Rev.* **81,** 93–134 (2007).
7. Thompson, R. S., Whitlock, C., Bartlein, P. J., Harrison, S. P. & Spaulding, W. G. in *Global Climates Since the Last Glacial Maximum* (eds Wright, H. E. Jr *et al.*) 468–513 (Univ. Minnesota Press, 1993).
8. Loutre, M. F. & Berger, A. *Global Planet. Change* **36,** 209–217 (2003).
9. Berger, A. & Loutre, M. F. *Science* **297,** 1287–1288 (2002).
10. Harrison, S. P. *et al. Clim. Dyn.* **20,** 663–688 (2003).
11. Siegenthaler, U. *et al. Science* **310,** 1313–1317 (2005).
12. Spahni, R. *et al. Science* **310,** 1317–1321 (2005).

LETTER

doi:10.1038/nature09839

Extended megadroughts in the southwestern United States during Pleistocene interglacials

Peter J. Fawcett[1], Josef P. Werne[2,4,5], R. Scott Anderson[6,7], Jeffrey M. Heikoop[8], Erik T. Brown[3], Melissa A. Berke[3], Susan J. Smith[7], Fraser Goff[1], Linda Donohoo-Hurley[1], Luz M. Cisneros-Dozal[8], Stefan Schouten[9], Jaap S. Sinninghe Damsté[9], Yongsong Huang[10], Jaime Toney[8], Julianna Fessenden[6], Giday WoldeGabriel[6], Viorel Atudorei[1], John W. Geissman[1] & Craig D. Allen[11]

The potential for increased drought frequency and severity linked to anthropogenic climate change in the semi-arid regions of the southwestern United States (US) is a serious concern[1]. Multi-year droughts during the instrumental period[2] and decadal-length droughts of the past two millennia[1,3] were shorter and climatically different from the future permanent, 'dust-bowl-like' megadrought conditions, lasting decades to a century, that are predicted as a consequence of warming[4]. So far, it has been unclear whether or not such megadroughts occurred in the southwestern US, and, if so, with what regularity and intensity. Here we show that periods of aridity lasting centuries to millennia occurred in the southwestern US during mid-Pleistocene interglacials. Using molecular palaeotemperature proxies[5] to reconstruct the mean annual temperature (MAT) in mid-Pleistocene lacustrine sediment from the Valles Caldera, New Mexico, we found that the driest conditions occurred during the warmest phases of interglacials, when the MAT was comparable to or higher than the modern MAT. A collapse of drought-tolerant C_4 plant communities during these warm, dry intervals indicates a significant reduction in summer precipitation, possibly in response to a poleward migration of the subtropical dry zone. Three MAT cycles ~2 °C in amplitude occurred within Marine Isotope Stage (MIS) 11 and seem to correspond to the muted precessional cycles within this interglacial. In comparison with MIS 11, MIS 13 experienced higher precessional-cycle amplitudes, larger variations in MAT (4–6 °C) and a longer period of extended warmth, suggesting that local insolation variations were important to interglacial climatic variability in the southwestern US. Comparison of the early MIS 11 climate record with the Holocene record shows many similarities and implies that, in the absence of anthropogenic forcing, the region should be entering a cooler and wetter phase.

The hydroclimatology of the southwestern US shows significant natural variability including major historical droughts[1]. Models of climate response to anthropogenic warming predict future dust-bowl-like conditions that will last much longer than historical droughts and have a different underlying cause, a poleward expansion of the subtropical dry zones[4]. At present, no palaeoclimatic analogues are available to assess the potential duration of aridity under a warmer climate or to evaluate its effect on the seasonality of precipitation.

Here we present a high-resolution climate record from an 82-m lacustrine sediment core (VC-3) from the Valles Caldera (Fig. 1) that spans two mid-Pleistocene glacial cycles from MIS 14 to MIS 10 (552 kyr ago to ~368 kyr ago; see Supplementary Information). MISs 11 and 13 are long interglacials that may have been as warm as

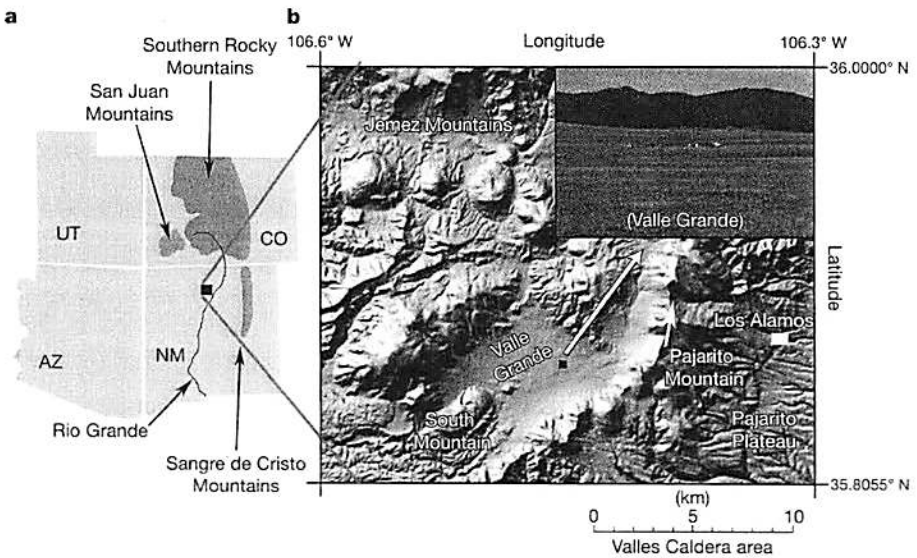

Figure 1 | Location map of the Valles Caldera. a, Location in northern New Mexico. b, Digital elevation model of the Valles Caldera showing the location of South Mountain rhyolite, Valle Grande, the drilling location of core VC-3 (black square) and a photograph of the drilling site.

[1]Department of Earth & Planetary Sciences, University of New Mexico, Albuquerque, New Mexico 87131, USA. [2]Large Lakes Observatory and Department of Chemistry and Biochemistry, University of Minnesota Duluth, Duluth, Minnesota 55812, USA. [3]Large Lakes Observatory and Department of Geological Sciences, University of Minnesota Duluth, Duluth, Minnesota 55812, USA. [4]Centre for Water Research, University of Western Australia, Crawley, Western Australia 6009, Australia. [5]WA-Organic and Isotope Geochemistry Centre, Curtin University of Technology, Bentley, Western Australia 6845, Australia. [6]School of Earth Sciences and Environmental Sustainability, Northern Arizona University, Flagstaff, Arizona 86011, USA. [7]Laboratory of Paleoecology, Bilby Research Center, Northern Arizona University, Flagstaff, Arizona 86011, USA. [8]Earth and Environmental Sciences Division, EES-14, Los Alamos National Laboratory, Los Alamos, New Mexico 87545, USA. [9]NIOZ Royal Netherlands Institute for Sea Research, Department of Marine Organic Biogeochemistry, PO Box 59, 1790 AB Den Burg, Netherlands. [10]Department of Geological Sciences, Brown University, Providence, Rhode Island 02912, USA. [11]USGS Fort Collins Science Center, Jemez Mountains Field Station, Los Alamos, New Mexico 87544, USA.

20. Bin-Omran, S., Kornev, I., Ponomareva, I. & Bellaiche, L. Diffuse phase transitions in ferroelectric thin films from first principles. *Phys. Rev. B* **81,** 094119 (2010).
21. Bousquet, E. *et al.* Improper ferroelectricity in perovskite oxide artificial superlattices. *Nature* **452,** 732–737 (2008).
22. Pertsev, N. A., Zembilgotov, A. G. & Tagantsev, A. K. Effect of mechanical boundary conditions on phase diagrams of epitaxial ferroelectric thin films. *Phys. Rev. Lett.* **80,** 1988–1991 (1998).
23. Lai, B.-K., Kornev, I., Bellaiche, L. & Salamo, G. Phase diagrams of epitaxial $BaTiO_3$ ultrathin films from first principles. *Appl. Phys. Lett.* **86,** 132904 (2005).
24. Lee, H. N., Christen, H. M., Chisholm, M. F., Rouleau, C. M. & Lowndes, C. H. Strong polarization enhancement in asymmetric three-component ferroelectric superlattices. *Nature* **433,** 395–399 (2004).
25. Lisenkov, S. & Bellaiche, L. Phase diagrams of $BaTiO_3/SrTiO_3$ superlattices from first principles. *Phys. Rev. B* **76,** 020102(R) (2007).
26. Walizer, L., Lisenkov, S. & Bellaiche, L. Finite-temperature properties of $(Ba,Sr)TiO_3$ systems from atomistic simulations. *Phys. Rev. B* **73,** 144105 (2006).
27. Sethna, J. P. Frustration, curvature and defect lines in metallic glasses and the cholesteric blue phase. *Phys. Rev. B* **31,** 6278–6297 (1985).
28. Vedmedenko, E. Y. *Competing Interactions in the Nanoworld* 3–16 (Wiley-VCH, 2007).
29. Narasimhan, S. & Vanderbilt, D. Elastic stress domains and the herringbone reconstruction on Au(111). *Phys. Rev. Lett.* **69,** 2455–2458 (1992).
30. Vanderbilt, D. in *Computations for the Nano-Scale* (eds Blöchl, P. E., Fisher, A. J. & Joachim, C.) 1–11 (Kluwer, 1993).

Supplementary Information is linked to the online version of the paper at www.nature.com/nature.

Acknowledgements This work was supported by the US National Science Foundation, Office of Naval Research and Department of Energy. We gratefully acknowledge extensive use of the supercomputing resources of the University of Arkansas High Performance Computing Center as well as the Center for Piezoelectrics by Design, College of William and Mary, Virginia. We thank A. Apon, D. Chaffin, J. Pummill and E. J. Walter for computational support.

Author Contributions This work is an outgrowth of an ongoing project on compositionally modulated ferroelectrics at the University of Arkansas. L.W., S.L. and L.B. developed an effective-Hamiltonian implementation for BST systems. N.C. carried out the present Monte Carlo simulations using these effective-Hamiltonian and code implementations. N.C. found exotic degenerate ground states and spiral domains and suggested that these complex results can be explained in terms of geometric frustration. L.B. proposed further studies of critical behaviours and size dependency, and these additional simulations were carried out by N.C. Various complex details were jointly analysed by N.C. and L.B. and together they wrote the paper, with feedback from L.W. and S.L.

Author Information Reprints and permissions information is available at www.nature.com/reprints. The authors declare no competing financial interests. Readers are welcome to comment on the online version of this article at www.nature.com/nature. Correspondence and requests for materials should be addressed to N.C. (narayani@uark.edu).

the Holocene epoch, and MIS 11 is a good analogue for future natural climate variability with similar, low-amplitude precessional cycles[6,7]. We used novel organic geochemical proxies (the cyclization ratio of branched tetraethers (CBT, related to pH) and the methylation index of branched tetraethers (MBT, related to temperature and pH[5,8])) to reconstruct the annual MAT of the Valles Caldera watershed, and compared these with proxies of hydrologic balance to evaluate the relationship between warmth and aridity.

Interglacial MATs in the VC-3 record range from ~0 to 7 °C, with the highest temperatures occurring in MIS 13 and early in MIS 11 (Fig. 2). The highest temperatures (5–7 °C) are similar to modern MATs, of ~5 °C. The glacial stages have multiple millennial-scale temperature oscillations with amplitudes as large as 7 °C; approximately seven oscillations are preserved in MIS 12 (B1–B7), three in late MIS 14 (C1–C3) and one in early MIS 10 (A1). The frequency of these oscillations (2–10 kyr) is similar to those recorded in contemporaneous Atlantic Ocean sediment records[9]. All VC-3 stadials correlate with high percentages of *Picea* + *Abies* pollen, whereas interstadials have lower *Picea* + *Abies* pollen percentages and many correlate with local maxima in *Juniperus* and *Quercus* (Fig. 2). Increased percentages of Cyperaceae (sedge) pollen during several interstadials suggest a shallower lake rimmed by a broad marshy zone, which would have been minimized during stadials, when the lake was deeper. Interstadial shallowing probably resulted from increased evaporation and/or a reduction in the winter precipitation that dominates regional glacial-stage precipitation[10].

Glacial terminations VI and V in the VC-3 record show temperature increases of ~7 and ~8 °C, respectively. The $\delta^{13}C$ record of TOC (Fig. 2) shows negative isotopic shifts of 2.5–3.5‰ at the terminations that we interpret as biotic responses to global increases in atmospheric CO_2, similar to the Termination I $\delta^{13}C$ response in Lake Baikal[11].

We subdivide MIS 11 into five distinct substages, three warm and two cool, on the basis of MAT estimates, warm (lower-elevation) versus boreal (higher-elevation) pollen taxa, and variation in aquatic productivity proxies (Fig. 2). The warm substages (MISs 11a, c and e) are separated by intervals in which the temperature is ~2 °C lower (MISs 11b and d). Although these small temperature variations are within the error limits of the MBT/CBT calibration, their timing is supported by decreases in warm pollen taxa and increases in boreal pollen taxa (with the exception of MIS 11a). The warmest substage, MIS 11e, occurs early in the interglacial, and has peak MATs of 6–7 °C and the highest percentages of *Juniperus* pollen. After MIS 11e, the warm substages become progressively cooler.

The preservation of five MIS 11 substages in VC-3 is unusual. Most published records recognize only three substages, although a weak MIS 11e was noted in the Lake Baikal biogenic silica record[12] and there are three distinct (warm) peaks in MIS 11 pollen influx from Greenland preserved in ODP Site 646 sediments[13]. The VC-3 MIS 11a substage is cooler than the extended warm phases of MIS 11, similar to other mid-Pleistocene climate records[12], and is defined mainly by elevated lacustrine productivity (Si/Ti and TOC), more-positive $\delta^{13}C$ values, slightly higher temperature estimates and a combination of *Quercus*, *Picea* and *Abies* pollen that may not have a good modern climatic analogue. Within the limits of the VC-3 age model and the calibration uncertainty in the MBT/CBT proxies, the warm substages seem to correspond to the three precessional peaks of MIS 11, suggesting that the temperature response of this region to low-amplitude precessional cycles is ~2 °C. On the basis of the MIS 11 orbital forcing similarity with the Holocene, we suggest that in the absence of anthropogenic forcing future southwestern US climate should see a cooling of ~2 °C relative to the early Holocene.

Large parts of MIS 13 seem to have been warmer than most of MIS 11, as shown by MATs of up to 7 °C, higher *Juniperus* pollen percentages and the absence of *Picea* + *Abies* pollen (Fig. 2). Only MIS 11e had temperatures approaching the peak warmth of MIS 13. Other Northern Hemisphere records suggest that MIS 13 was warmer than

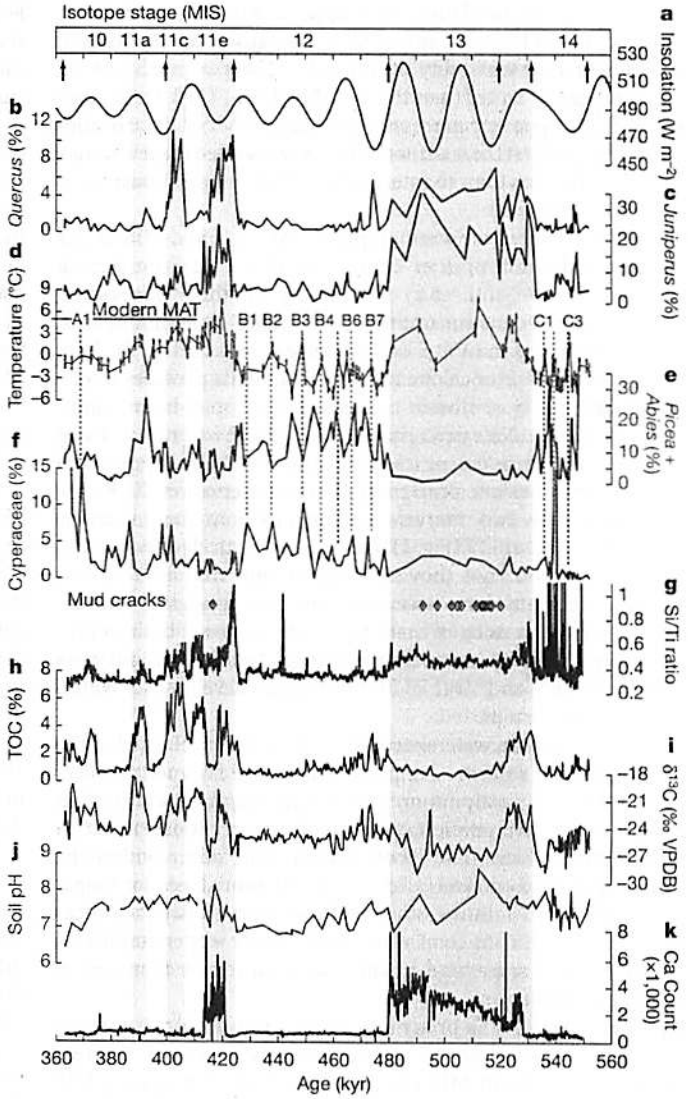

Figure 2 | Multi-proxy profiles of VC-3 plotted versus calendar age. Age model age–depth tie points are shown as arrows at the top and possible sedimentary hiatuses are indicated by positions of mud cracks (below). Shading indicates interglacial periods including odd-numbered MISs 11 and 13 and substages within MIS 11 (a, c and e). **a**, June insolation at latitude 30° N (ref. 6). **b**, *Quercus* (warm) pollen percentages. **c**, *Juniperus* (warm) pollen percentages. **d**, MAT estimates from MBT/CBT, with data size marker equivalent to 2 °C (blue). Red line shows the modern MAT, of 4.8 °C, in the Valle Grande. MBT/CBT temperature estimates have an absolute uncertainty of 5 °C based on uncertainties in the global calibration (see further discussion in Supplementary Information). Millennial-scale events within the three glacial periods, defined by local maxima in MAT and Cyperaceae and local minima in *Picea* and *Abies*, are indicated (A for MIS 10, B for MIS 12 and C for MIS 14). **e**, *Picea* + *Abies* (boreal) pollen percentages. **f**, Cyperaceae pollen percentages; mud cracks indicated with orange diamonds. **g**, Si/Ti ratios from core scanning X-ray fluorescence (XRF). Large peaks in MIS 14 correspond to pumiceous gravels. **h**, Total organic carbon (TOC). **i**, $\delta^{13}C_{TOC} = ((^{13}C/^{12}C)_{sample}/(^{13}C/^{12}C)_{standard} - 1) \times 1{,}000‰$, relative to the Vienna PeeDee Belemnite (VPBD) standard. **j**, Watershed soil pH estimate from CBT. **k**, Calcium concentration in sediments from core scanning XRF.

MIS 11[14,15], and a smaller Greenland ice sheet[13] and a lack of ice rafting in the North Atlantic[9] also indicate Northern Hemisphere warmth during MIS 13, although not necessarily more than during MIS 11. In contrast, Southern Hemisphere records uniformly show a cooler MIS 13[14,16].

The higher MIS 13 temperatures in the southwestern US occur despite lower interglacial values of atmospheric CO_2 and CH_4 (ref. 17). However, the amplitude of precessional cycles and, hence, extremes in

Northern Hemisphere insolation were larger in MIS 13 than MIS 11[6] and may have led to higher continental temperatures during parts of MIS 13. Temperature variability during MIS 13 was as much as 6 °C, which is significantly larger than that during MIS 11 (Fig. 2). In combination with the apparent precessional timing of MIS 11 warm substages, this suggests that the southwestern US responded more strongly to insolation variations than to interglacial trends in greenhouse gases or global ice volume.

Mud cracks present in the warmest phases, MIS 11e and MIS 13, are unambiguous indicators of drier conditions. One 70-cm mud crack occurs within MIS 11e, and ~3 m of section within the upper portion of MIS 13 sediments contains multiple, centimetre-scale mud cracks, making this portion of the VC-3 age model less certain (Fig. 2). Also, the presence or absence of calcite in VC-3 sediments provides a continuous indicator of closed-basin or, respectively, open-basin conditions in the lake. No calcite precipitated during freshwater open-basin conditions, whereas during drier (closed-basin) conditions, evaporative concentration led to calcite precipitation and preservation. XRF core scanning results show two intervals with high calcium concentrations during MISs 11e and MIS 13 (Fig. 2) that correlate with elevated (1–2%) total inorganic carbon (not shown), whereas core sections with low calcium concentrations have essentially no total inorganic carbon. Significant increases in calcium mark the onsets of closed-basin conditions coincident with rapid temperature increases a few thousand years after Terminations V and VI (Fig. 2). Mud cracks develop later within these closed-basin periods.

Long-term changes in watershed hydrology are also reflected in the CBT-derived soil pH record. Changes in soil pH are assumed to reflect changes in total precipitation[18]; greater soil leaching and acidification occurs with more precipitation, whereas drier conditions result in weaker soil acidification. The most alkaline soils occur within the interglacial mud-cracked facies (Fig. 2) and are more basic for longer periods in MIS 13. In contrast, soil pH shows a progressive acidification through MIS 12, consistent with progressively wetter conditions through that glacial stage, and possibly also caused by increases in boreal tree vegetation.

During MIS 11e, Si/Ti (a proxy for diatom productivity) is initially very high and then declines to average interglacial values, whereas TOC increases to ~5% in MIS 11e and is also high during early MIS 11d and MISs 11c and 11a. After the glacial termination, $\delta^{13}C_{TOC}$ rapidly increases to ~−20‰, indicating an expansion of C_4 plants in the watershed and higher lacustrine productivity levels[19]. Increases $\delta^{13}C_{TOC}$ also occurs in MISs 11c and 11a, and early in MIS 11d. Continued high Si/Ti, TOC and more-positive $\delta^{13}C_{TOC}$ values during early stages of closed-basin conditions in MIS 11e and MIS 13 indicate periods of robust summer precipitation and productivity related to insolation forcing of monsoon strength, even as reduced winter precipitation led to less precipitation overall and closed-basin conditions.

Mud-cracked facies in MIS 11e and MIS 13 are characterized by negative shifts in $\delta^{13}C_{TOC}$ of 6–7‰ and dramatic decreases in percentage TOC (Fig. 2). Si/Ti ratios, however, remain elevated relative to glacial values, suggesting that low percentage TOC values are due to organic degradation in shallow, oxidized sediments rather than lower aquatic productivity. The large negative shifts in $\delta^{13}C_{TOC}$ are best explained by a collapse of the interglacial C_4 plant community. Variations in C_3 and C_4 plant communities are a complex function of temperature, atmospheric CO_2, and growing-season precipitation[20,21]. These dry intervals include some of the highest MATs in the VC-3 record that should favour C_4 plants, and the relatively high interglacial levels of atmospheric CO_2 during MISs 11 and 13 vary by less than 20–30 p.p.m.v. Thus, the best explanation for the decline of C_4 plants in the watershed is a significant decrease in summer precipitation. In contrast to the early interglacial closed-basin phases where significant C_4 plant growth provided evidence for robust summer precipitation, we interpret the extended arid periods later in MIS 11e and MIS 13 to be the result of greatly reduced summer precipitation. Following the aridity of MIS 11e, the lake expanded during MIS 11d as shown by well-laminated sediments and open-basin conditions (low calcium values). Despite this interval being ~2 °C cooler, sufficient summer rainfall early in MIS 11d allowed renewed C_4 plant growth.

Northern New Mexico at present receives ~40–50% of its annual precipitation total during the summer monsoon[22]. During the warmest phases of the interglacials, we would expect greater summer precipitation, as the monsoon is primarily driven by land surface heating[22]. Indeed, linkages among interglacial warmth, robust summer precipitation and precessional variations are indicated by the presence of C_4 plants in early MIS 13, early MIS 11e and MISs 11c and 11a, when MATs were similar to or slightly less than modern values, but the warmest intervals did not have robust summer precipitation. As possible analogues for interglacial aridity, both historical droughts and pre-historical megadroughts were characterized by reductions in winter precipitation as a consequence of more-frequent La Niña events2[2,3,23], with summer precipitation reduced also.

In contrast, the extended arid episodes (centuries to millennia) of MIS 11e and MIS 13 lasted much longer than pre-historical megadroughts. An analogous relationship between peak interglacial warmth and extended aridity was also noted in a mid-Holocene bog record from the margin of the Valles Caldera[24]. Here, ~2 kyr of desiccation occurred contemporaneously with the highest temperatures of the Holocene in the southwestern US[25] and with the northernmost extent of the intertropical convergence zone in the Gulf of Mexico[26]. The timing of this dry episode in the Holocene interglacial following the deglaciation is very similar to that of the arid episode in MIS 11e; subsequent late-Holocene conditions became wetter in the southwestern US, with increased winter precipitation[27] similar in timing to wetter conditions during MIS 11d in the VC-3 record.

The strong correspondence between the warmest temperatures and extended aridity during at least three interglacials (MIS 13, MIS 11e and the early Holocene) in the southwestern US suggests a stable climate state fundamentally different from conventional drought conditions. These periods of aridity are related to lower winter precipitation (as mid-latitude westerlies shifted polewards during warmer periods), but reductions in summer precipitation seem to be critical to their development. Unlike the temporary summer blocking high over the southwestern US thought to partly explain the 1950s drought[28], these longer periods of aridity indicate a more permanent change in atmospheric circulation. Climate model analysis shows that the dust-bowl-like conditions predicted for the southwestern US over the next century in response to anthropogenic warming arise from a poleward shift of the mid-latitude westerlies and the poleward branch of the Hadley cell[4]. This response to warming is not transient and would result in a more arid southwestern US as long as the underlying conditions (warming) remained in place. Our palaeoclimate record shows that extended interglacial aridity is strongly linked to higher-than-modern temperatures and reduced summer rainfall, and we suggest that a similar expansion of the subtropical dry zone has occurred several times in the past in response to natural warming, even though MIS 11 and MIS 13 had different orbital and atmospheric CO_2 forcings. Our results strongly indicate that interglacial climates in the southwestern US can experience prolonged periods of aridity, lasting centuries to millennia, with profound effects on water availability and ecosystem composition. The risk of prolonged aridity is likely to be heightened by anthropogenic forcing[1,4].

METHODS SUMMARY

Measurement of fossil branched glycerol dialkyl glycerol tetraether (GDGT) membrane lipids from soil bacteria were conducted at the Royal Netherlands Institute for Sea Research (NIOZ) and Brown University following procedures outlined in Supplementary Information. At NIOZ we analysed GDGTs on an Agilent 1100 series LC-MSD SL, and at Brown University we analysed GDGTs on an HP 1200 series LC-MS. Both labs used an Alltech Prevail Cyano column (2.1 × 150 mm, 3 μm) with the same solvent elution scheme and instrument operating conditions. GDGTs were detected using atmospheric-pressure chemical ionization mass spectrometry. All

liquid chromatography/mass spectrometry runs were integrated at NIOZ by the same technician to ensure consistency. To evaluate the compatibility between the Brown and NIOZ measurements, representative samples were analysed on both machines and the resulting MBT/CBT indices were found to be identical within analytical uncertainty.

Processing for pollen included suspension in KOH, dilute HCL, hydrofluoric acid and acetolysis solution. The pollen sum included all terrestrial pollen types; Cyperaceae percentages were calculated outside the sum. We identified pollen grains to the lowest taxonomic level using the modern pollen reference collection at Northern Arizona University. Analysis for organic carbon elemental concentrations and $\delta^{13}C_{TOC}$ included samples being dried, ground and pretreated twice with 6 N HCL at 60 °C to remove the carbonate fraction. TOC and $\delta^{13}C_{TOC}$ were analysed using a Costech Elemental Analyser coupled to a Thermo-Finnigan Delta Plus isotope ratio mass spectrometer. The bulk elemental composition of core VC-3 sediments was determined using an ITRAX X-ray Fluorescence Scanner (Cox Analytical Instruments). XRF scanning was conducted at 1-cm resolution with 60-s scans using a molybdenum X-ray source set to 30 kV and 15 mA.

Received 11 June 2010; accepted 12 January 2011.

1. Woodhouse, C. A. *et al.* A 1,200-year perspective of 21st century drought in southwestern North America. *Proc. Natl Acad. Sci. USA* **107,** 21283–21288 (2010).
2. McCabe, G. J., Palecki, M. A. & Betancourt, J. L. Pacific and Atlantic Ocean influences on multidecadal drought frequency in the United States. *Proc. Natl Acad. Sci. USA* **101,** 4136–4141 (2004).
3. Cook, E. R., Seager, R., Cane, M. A. & Stahle, D. W. North American drought: reconstructions, causes and consequences. *Earth Sci. Rev.* **81,** 93–134 (2007).
4. Seager, R. *et al.* Model projections of an imminent transition to a more arid climate in southwestern North America. *Science* **316,** 1181–1184 (2007).
5. Weijers, J. W. H., Schouten, S., van den Donker, J. C., Hopmans, E. C. & Sinninghe Damsté, J. S. Environmental controls on bacterial tetraether membrane lipid distribution in soils. *Geochim. Cosmochim. Acta* **71,** 703–713 (2007).
6. Berger, A. & Loutre, M. F. Insolation values for the climate of the last 10 million years. *Quat. Sci. Rev.* **10,** 297–317 (1991).
7. Loutre, M. F. & Berger, A. Marine Isotope Stage 11 as an analog for the present interglacial. *Global Planet. Change* **36,** 209–217 (2003).
8. Weijers, J. W. H., Schefuß, E., Schouten, S. & Sinninghe Damsté, J. S. Coupled thermal and hydrological evolution of tropical Africa over the last deglaciation. *Science* **315,** 1701–1704 (2007).
9. McManus, J. F., Oppo, D. W. & Cullen, J. L. A 0.5-million-year record of millennial-scale climate variability in the North Atlantic. *Science* **283,** 971–975 (1999).
10. Kutzbach, J. E. *et al.* Climate and biome simulation for the past 21000 years. *Quat. Sci. Rev.* **17,** 473–509 (2000).
11. Prokopenko, A. A., Williams, D. F., Karabanov, E. B. & Khursevich, G. K. Response of Lake Baikal ecosystem to climate forcing and pCO_2 change over the Last Glacial/Interglacial transition. *Earth Planet. Sci. Lett.* **172,** 239–253 (1999).
12. Prokopenko, A. A. *et al.* Muted climate variations in continental Siberia during the mid-Pleistocene epoch. *Nature* **418,** 65–68 (2002).
13. de Vernal, A. & Hillaire-Marcel, C. Natural variability of Greenland climate, vegetation, and ice volume during the past million years. *Science* **320,** 1622–1625 (2008).
14. Guo, Z. T., Berger, A., Yin, Q. Z. & Qin, L. Strong asymmetry of hemispheric climates during MIS-13 inferred from correlating China loess and Antarctic ice records. *Clim. Past* **5,** 21–31 (2009).
15. Rossignol-Strick, M., Paterne, M., Bassinot, F. C., Emeis, K. C. & De Lange, G. J. An unusual mid-Pleistocene monsoon period over Africa and Asia. *Nature* **392,** 269–272 (1998).
16. Jouzel, J. *et al.* Orbital and millennial Antarctic climate variability over the past 800,000 years. *Science* **317,** 793–796 (2007).
17. Loulergue, L. *et al.* Orbital and millennial-scale features of atmospheric CH_4 over the past 800,000 years. *Nature* **453,** 383–386 (2008).
18. Johnson, D. W., Hanson, P. J., Todd, D. E., Susfalk, R. B. & Trettin, C. F. Precipitation change and soil leaching: field results and simulations from Walker Branch Watershed, Tennessee. *Wat. Air Soil Pollut.* **105,** 251–262 (1998).
19. Meyers, P. A. Applications of organic geochemistry to paleolimnological reconstructions: a summary of examples from the Laurentian Great Lakes. *Org. Geochem.* **34,** 261–289 (2003).
20. Ehleringer, J. R., Cerling, T. E. & Helliker, B. R. C_4 photosynthesis, atmospheric CO_2 and climate. *Oecologia* **112,** 285–299 (1997).
21. Huang, Y. *et al.* Climate change as the dominant control on glacial-interglacial variations in C_3 and C_4 plant abundance. *Science* **293,** 1647–1651 (2001).
22. Douglas, M. W., Maddox, R. A., Howard, K. & Reyes, S. The Mexican monsoon. *J. Clim.* **6,** 1665–1677 (1993).
23. Schubert, S. D., Suarez, M. J., Pegion, P. J., Koster, R. D. & Bacmeister, J. T. On the cause of the 1930s dust bowl. *Science* **303,** 1855–1859 (2004).
24. Anderson, R. S. *et al.* Development of the mixed conifer forest in northern New Mexico and its relationship to Holocene environmental change. *Quat. Res.* **69,** 263–275 (2008).
25. Jiménez-Moreno, G., Fawcett, P. J. & Anderson, R. S. Millennial- and centennial-scale vegetation and climate changes during the Late Pleistocene and Holocene from northern New Mexico (USA). *Quat. Sci. Rev.* **27,** 1448–1452 (2008).
26. Poore, R. Z., Pavich, M. J. & Grissino-Mayer, H. D. Record of the North American southwest monsoon from Gulf of Mexico sediment cores. *Geology* **33,** 209–212 (2005).
27. Enzel, Y., Cayan, D. R., Anderson, R. Y. & Wells, S. G. Atmospheric circulation during Holocene lake stands in the Mojave Desert: evidence of regional climate change. *Nature* **341,** 44–47 (1989).
28. Namias, J. Some meteorological aspects of drought with special reference to the summers of 1952–54 over the United States. *Mon. Weath. Rev.* **83,** 199–205 (1955).

Supplementary Information is linked to the online version of the paper at www.nature.com/nature.

Acknowledgements We thank A. Mets for analytical support, W. McIntosh for the Ar–Ar age determination, T. Wawrzyniec and A. Ellwein for drilling help, and the Valles Caldera Trust for permission to drill in the Valle Grande. Core assistance was provided by LRC/LacCore. This work was supported by the NSF Paleoclimate and P2C2 programs, IGPP LANL and the USGS Western Mountain Initiative. Support from the Gledden Fellowship is acknowledged. This work forms contribution 2399-JW at the Centre for Water Research, The University of Western Australia and contribution 131 at the Laboratory of Paleoecology, Northern Arizona University.

Author Contributions Writing and interpretation was done by P.J.F. with significant contributions from J.P.W., R.S.A., J.M.H. and E.T.B. MBT/CBT analyses were conducted by J.P.W., M.A.B., J.S.S.D., S.S., Y.H. and J.T. Organic carbon/nitrogen analyses were conducted by P.J.F., J.M.H., L.M.C.-D., J.F. and V.A. XRF core scanning analyses were conducted by E.T.B. Pollen analyses and palaeovegetation analyses were conducted by R.S.A., S.J.S. and C.D.A., and F.G., G.W. and P.J.F. conducted core sediment and stratigraphic analyses. L.D.-H. and J.W.G. investigated palaeomagnetic and rock magnetic core properties. All authors discussed the results and commented on the manuscript.

Author Information Reprints and permissions information is available at www.nature.com/reprints. The authors declare no competing financial interests. Readers are welcome to comment on the online version of this article at www.nature.com/nature. Correspondence and requests for materials should be addressed to P.J.F. (fawcett@unm.edu).

LETTER

doi:10.1038/nature09828

Seismic tremors and magma wagging during explosive volcanism

A. Mark Jellinek[1] & David Bercovici[2]

Volcanic tremor is a ubiquitous feature of explosive eruptions. This oscillation persists for minutes to weeks and is characterized by a remarkably narrow band of frequencies from about 0.5 Hz to 7 Hz (refs 1–4). Before major eruptions, tremor can occur in concert with increased gas flux and related ground deformation[5–7]. Volcanic tremor is thus of particular value for eruption forecasting[6,8]. Most models for volcanic tremor rely on specific properties of the geometry, structure and constitution of volcanic conduits as well as the gas content of the erupting magma. Because neither the initial structure nor the evolution of the magma-conduit system will be the same from one volcano to the next, it is surprising that tremor characteristics are so consistent among different volcanoes. Indeed, this universality of tremor properties remains a major enigma. Here we employ the contemporary view that silicic magma rises in the conduit as a columnar plug surrounded by a highly vesicular annulus of sheared bubbles[9,10]. We demonstrate that, for most geologically relevant conditions, the magma column will oscillate or 'wag' against the restoring 'gas-spring' force of the annulus at observed tremor frequencies. In contrast to previous models, the magma-wagging oscillation is relatively insensitive to the conduit structure and geometry, which explains the narrow band of tremor frequencies observed around the world. Moreover, the model predicts that as an eruption proceeds there will be an upward drift in both the maximum frequency and the total signal frequency bandwidth, the nature of which depends on the explosivity of the eruption, as is often observed.

The main characteristics of volcanic tremor depend strongly on whether a volcano is erupting explosively and on the intensity of the event (Fig. 1). Long before an eruption, tremor is 'narrow-band' (about 0.5–2 Hz and sometimes monochromatic or harmonic). On transitions to active volcanism, however, the maximum frequency can climb to 5–7 Hz (refs 1–4) (Fig. 1c and d). Moreover, whereas tremor related to low-intensity volcanism remains narrow-band, tremor associated with intermittent or protracted explosive behaviour is 'broadband', characterized by power distributed over the full ~0.5–7 Hz tremor bandwidth.

A successful model for volcanic tremor must ultimately explain its excitation, longevity and restricted frequency bandwidth, as well as its evolution in spectral character over changes in eruption style (Fig. 1). Such an endeavour is difficult because the signal can include contributions from the source region ('source effects') and the magma-filled conduit system through which seismic waves propagate ('path effects')[1,11–13]. Previous modelling efforts suggest that tremor can be driven and modulated by processes related to time-dependent mechanical coupling of ascending magma to the conduit walls[14,15], unsteady stirring in a gas-rich magma[8,16,17], and the interaction of ascending magma with irregularities in the conduit diameter and wall structure, such as constrictions[18] and cracks[8,19].The initial signal bandwidth and its upward drift with volcanism might be related to time-varying path effects, such as the gas content, bubble size distribution and bubble nucleation depth in the magma, as well as the height and average diameter of the conduit[1,11–13,17]. Alternatively, time-dependent source effects—including the location, shape and structure of cracks of various class within the conduit walls, which act as 'resonators'[1,20], and the depth of seismicity related to brittle failure in the magma itself[14,21,22]—may influence the signal at the surface. A challenge for these models is that the structure and constitution of magma-conduit systems need not be similar from one volcano to the next before or during an eruption. Indeed, differences among the styles of conduit erosion[4,23] and magma degassing[9] would be predicted to produce large variations in the tremor signal bandwidth that are not observed (Fig. 1). In addition, it is not clear why the signal climbs in frequency but remains almost harmonic for low-energy events whereas it becomes broadband on transitions to Vulcanian or Plinian eruptive styles (Fig. 1).

Although the magma-conduit system may vary among volcanoes, for silica-rich magmas characteristic of explosive systems, experiments and calculation show that the magma—a mixture of very viscous melt, crystals and bubbles—rises as a stiff columnar plug that is highly sheared by viscous drag at the conduit walls[10]. In these systems bubbles and crystals do not move relative to the melt and impart a strain-rate-dependent rheology to the magma mixture[10]. In particular, depending on the gas content of the magma, shear strains are localized near the walls as a result of the preferential deformation of essentially inviscid bubbles, which causes the magma to flow as a plug. The depth H over which a plug flow is appropriate depends on the crystal content and the concentration and solubility of volcanic gas (primarily H_2O) and is of the order of a kilometre[10,24]. A key consequence of this plug flow is that the zone of sheared bubbles at the conduit wall develops into a thin, highly vesicular, permeable and compressible 'annulus' enveloping a 'stiff' central magma plug (Fig. 2)[9,10,25,26]. Textural analyses of pumice from effusive and explosive eruptions[27,28] show that the sheared and elongated bubbles within the annulus form a partially connected tube-like network with porosity ϕ_o of 30–90% (Fig. 2). Thus, the annulus is also permeable[27,28], so that gas can ascend relative to the magma column near the conduit wall[9,25]. Indeed, observations of rings of gas rising around the edges of active volcanic vents[26] (Fig. 2) suggest the presence of such a permeable annulus through which gas is transported.

Given the magma column–annulus structure, volcanic tremor would be a plausible consequence of the magma column rattling or wagging inside the bubble-rich annulus. In particular, lateral displacements of the column from a resting position in the centre of the conduit will compress or dilate the annulus, depending on which way the column is displaced. The annulus is essentially a semi-permeable springy foam that acts to restore the magma column to its resting position; however, the column's inertia causes it to overshoot that position, in which case an oscillation emerges and the column 'wags' back and forth. The corresponding gas-pressure fluctuations in the annulus are transmitted to the walls, giving rise to the tremor observed with seismometers and infrasound sensors at the surface.

A theoretical model describing a magma column oscillating within a compressible annulus is presented in the Supplementary Information. The essential physics of magma wagging is, however, captured by a

[1]Department of Earth and Ocean Sciences, The University of British Columbia, Vancouver, British Columbia, V6T 1Z4, Canada. [2]Department of Geology & Geophysics, Yale University, New Haven, Connecticut 06511, USA.